J Mater Sci (2007) 42:5826–5834
DOI 10.1007/s10853-006-1386-8

Experimental and numerical study of elastic behavior of heterogeneous model materials with spherical inclusions

N. Tessier-Doyen · J. C. Glandus · M. Huger

Received: 6 April 2004 / Accepted: 10 February 2006 / Published online: 24 May 2007
© Springer Science+Business Media, LLC 2007

Abstract The elastic properties of multi-phased materials have been studied in many papers, mainly focused on the analytical aspect of the problem (Voigt, Reuss, Hashin and Shtrikman...). For a few years, the large diffusion of FEM software offers, beside the analytical and experimental approaches, a new popular way to characterize the behavior laws of such materials. This work deals with two-phase model materials (spherical alumina inclusions in a vitreous matrix) whose linear elastic behaviors were determined by using the three previous approaches: analytical, experimental and numerical. Samples were elaborated with both various and controlled contents in second phase. The process consisted in determining their overall elastic characteristics starting from numerical 2D models, respecting the stereological relationships used in image analysis. After validation by comparison of the values obtained using four FEM software, the results were confronted with those given by analytical models so as with experimental ones. For the studied materials, experimental and numerical results are close to the lower bound of the Hashin and Shtrikman's model.

N. Tessier-Doyen · J. C. Glandus (✉) ·
M. Huger
ENSCI, GEMH, Limoges 87065, France
e-mail: jc_glandus@ensci.fr

Introduction

The macroscopic properties of coarse-grained multiphased materials such as concretes and other refractory products are often difficult to predict by using the well known analytical methods. In fact, their overall thermomechanical behavior (elastic and thermal properties) involves the influence of each component [1] so as their mutual interactions. Indeed, it becomes quickly very difficult to take into account both their intrinsic composition (nature and numbers of constituents), their microstructure (shape and spatial grains distribution) and their inherent defects (pores, cracks or decohesions).

The numerical simulation, which has more extended possibilities, appears as another way to predict the effective behavior of a multi-phased material on the basis of the behavior of its components. This work proposes a 2D simulation taking into account the stereological relationships dealing with the passage of a 3D system towards any 2D cut. The representativeness of the real material microstructure is thus respected in the plane used for calculation [2].

In a first stage, only materials with simplified microstructure and composition were studied. The objective was to investigate room temperature elastic properties of two-phase model materials constituted of two solid phases (one being randomly dispersed in the other) on a large range of content. The lack of decohesions at the interface inclusion/matrix was obtained thanks to the small thermal expansion mismatch between each component. Results of numerical modeling were compared both with the most current analytical models and with experimental

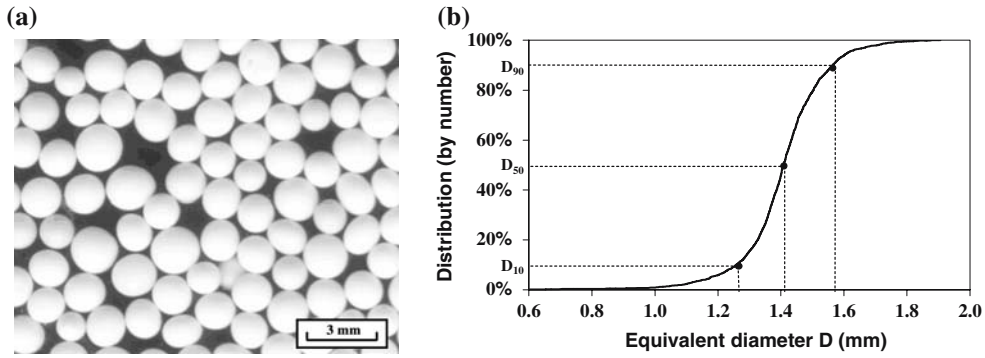

Fig. 1 Alumina balls: (**a**) scanned observation, (**b**) particle size distribution

values measured by ultrasonic waves propagation in order to validate the present approach.

To-phase material elaboration

The studied materials consist of spherical alumina particles, randomly distributed within a vitreous matrix, the quantities of second phase being perfectly controlled. To avoid significant interface decohesion, constituents with quite similar thermal expansion coefficients have been chosen (6.5×10^{-6} for the matrix and 7.7×10^{-6} K^{-1} for the balls in the temperature range 20–400 °C). Moreover, in order to facilitate further visual observations, the matrix exhibits a dark color which insures a good optical contrast with the white inclusions. The particle size distribution (by number) evaluated by image analysis shows an average particle diameter of 1.41 mm (Fig. 1).

The different stages of the process which leads to model materials with spherical inclusions are summarized in Fig. 2. First, glass matrix powder (average particle size: 7 μm) is dry mixed with the binder [cellulose ether], the plasticizer [polyethyleneglycol] and the lubricant [oleic acid]. Then a controlled fraction of alumina beads is added to the powder/binder mix whose basic recipe (Table 1) was developed for a 55 vol% of inclusions. Water-soluble organic additives used in the processing give to the mixture suitable rheological properties for cold uniaxial pressing (80 MPa) and increase the homogeneity of spatial distribution. After drying, green samples ($80 \times 40 \times 10$ mm) are put in a furnace for binder removing (0.3 °C min^{-1}, 450 °C, 4 h) and sintering. After 1 h at 680 °C (50 °C over the softening point of the matrix) in oxidant atmosphere and cooling down at room temperature, they are cut in bars ($50 \times 10 \times 10$ mm). A polished sample is shown in Fig. 3a: the dark phase corresponds to vitreous matrix and the lighter one to sections of alumina particles. To remove matrix porosity (Fig. 3b), post-hot pressing is carried out at 750 °C under 10 MPa pressure for 2 min. Final samples contain randomly distributed balls with low matrix porosity (Fig. 3c). Figure 3d shows both interfacial agreement between the two constituents and a small quantity of spherical closed porosity exhibited by alumina inclusions. For present materials, volumic fractions of the second phase range from 0 vol% to 55 vol%.

Experimentals

Evaluation of the volumic fraction of inclusions

By polishing each face of the thermo-compressed samples one can see the alumina balls sections (Fig. 3a). The surfacic content in circular sections is measured by image analysis: pictures of the four lateral faces of each bar are scanned (1,200 ppi) in gray levels. The subsequent pictures data processing is facilitated by the good color contrast between the balls and the matrix. The surfacic content s_p is given by the ratio between the surface area developed by the ball sections and the whole investigated surface area (balls + matrix). According to the stereological relationships dealing with the 2D/3D conformity of a two-phase system, the measured average surfacic content is

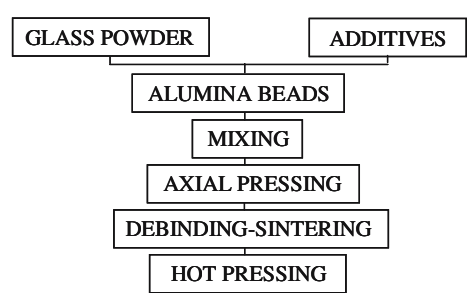

Fig. 2 Processing of alumina balls/glass materials

Table 1 Basic recipe of matrix powder/binder mix

Compound		Vol%
Glass powder	–	78
Methyl cellulose	Cellulose ether, Prolabo	6
Polyethylene glycol	PEG 300, Prolabo	2
Oleic acid	Zschimmer and Schwarz	1
Water	–	13

very close to the imposed volumic content v_p: the variation (s_p–v_p) is lower than 2% (Table 2). So the observed field can be considered, from a statistically standpoint, as a faithful representation of the 3D material.

Density measurements were performed by hydrostatic weighing. The experimental and theoretical densities exhibit comparable values (Table 2) which indicates that the matrix porosity of samples remains less than 1% after the hot pressing stage.

Young's modulus measurement at room temperature

Young's modulus measurement of two-phase materials

The ultrasonic waves propagation in the "infinite medium mode" with contact transducers has been used to determine Young's modulus of materials. In order to limit the attenuation, measurements were performed in transmission at low frequency (1 MHz). The time delay τ between the two echoes, determined by intercorrelation [3], corresponds to the travel time of the wave in the sample. Young's modulus is calculated by using both the transit duration of ultrasonic waves (τ_L for longitudinal waves, τ_T for transversal waves) and the apparent material density:

$$V_L = \frac{e}{\tau_L} \tag{1}$$

$$V_T = \frac{e}{\tau_T} \tag{2}$$

$$E_{exp} = \rho \cdot \frac{3 \cdot V_L^2 - 4 \cdot V_T^2}{\left(\frac{V_L}{V_T}\right)^2 - 1} \tag{3}$$

In order to obtain significant values over the whole sample, several measurements are carried out on various zones. The scattering of experimental values is 3.5% and the measured Young's modulus increases with the inclusion content (Table 3). This technique has also been used to estimate elastic properties of the

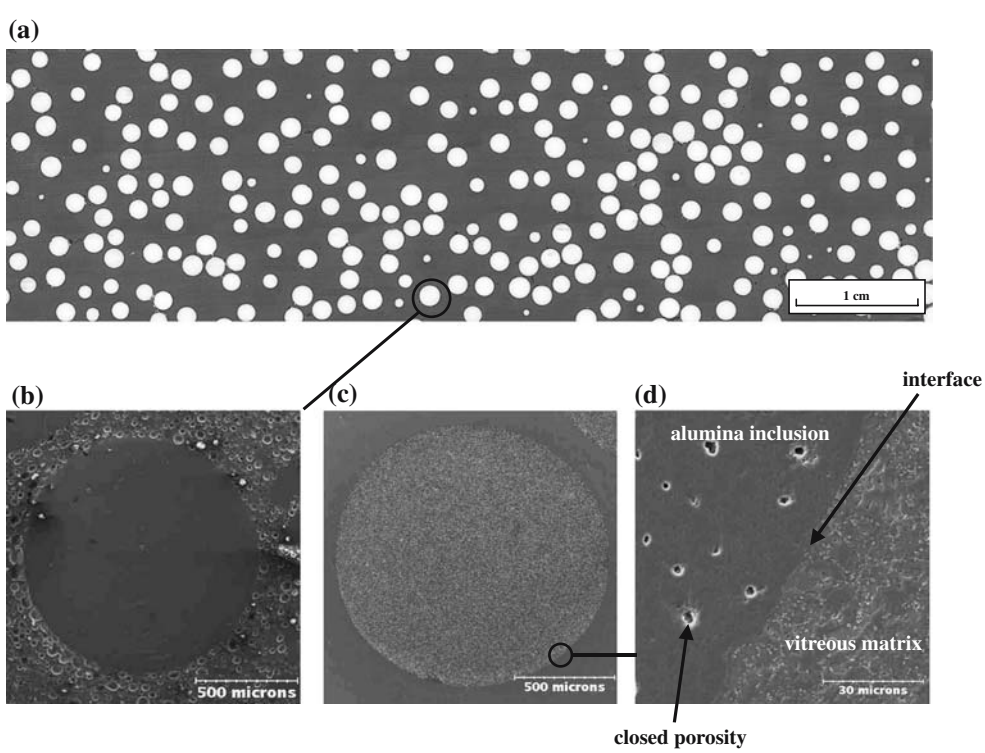

Fig. 3 Example of polished sample before and after hot-pressing treatment: (**a**) overall scanned sample, (**b**) matrix porosity before hot pressing treatment, (**c**) dense matrix after hot pressing treatment, (**d**) closed porosity in alumina inclusions and interfacial zone

Table 2 Comparison between surfacic and volumic contents, experimental and theoretical densities of alumina balls/glass materials

Sample gradation	s_p^* (%)	v_p^{**} (%)	s_p–v_p (%)	ρ(g cm^{-3}) Bulk	Theor.*	% Theor. density
0	0	0	0	2.757	2.760	99.9
1	5.3	5.0	0.3	2.787	2.792	99.8
2	8.6	7.5	1.1	2.794	2.807	99.5
3	11.9	13.0	–1.1	2.821	2.842	99.3
4	21.3	20.0	1.3	2.910	2.886	100.8
5	27.6	28.0	–0.4	2.931	2.936	99.8
6	35.7	35.0	0.7	2.982	2.981	100.0
7	48.9	45.0	1.9	3.051	3.056	99.8
8	54.2	55.0	–0.8	3.072	3.096	99.2

* Alumina surfacic fraction measured by image analysis

** Alumina balls volumic content of samples

*** Overall theoretical density estimated using density of 3.39 g cm^{-3} for alumina balls

matrix alone (78 GPa for the Young's modulus and 0.21 for the Poisson's ratio).

Young's modulus measurement of alumina balls

The Young's modulus of inclusions was measured by an ultrasonic immersion technique. Since the sample diameter is small and the acoustic attenuation remains low, the measurements were performed in reflection at high frequency (80 MHz). The transversal velocity cannot be obtain in this case, so Young's modulus was calculated (Eq. 4) assuming that Poisson's ratio equals 0.24, which is a standard value for such ceramic materials [4].

$$E = \rho \cdot V_L^2 \cdot \frac{(1-\nu)\cdot(1-2\nu)}{(1-\nu)} \tag{4}$$

In order to validate this assumption, a pure fine-grained alumina was used as reference standard (Degussit AL23). The measured average Young's modulus was about 390 GPa according to values commonly found in literature [5]. Moreover, 15 beads were randomly selected then ground in order to obtain two parallel faces distant of 0.8–1.3 mm. Measurement leads to experimental E results ranging between 220 GPa and 260 GPa. This value of 240 ± 20 GPa appears rather low compared with the elastic modulus of the AL23 material: it is attributable both to SiO_2, CaO, MgO and Na_2O impurities, identified by chemical analysis, and closed porosity showed previously in Fig. 3d. Besides, the scattering in measured values indicates that porosity can vary from one ball to another.

Analytical and numerical approaches

Analytical models

Many theoretical approaches have been developed to predict the overall elastic properties of multiphased materials. Parallel and serial arrangements of phases, assuming respectively uniform and continuous strain and stress were proposed by Voigt [6] and Reuss [7]. Hashin [8] introduced additional microstructural data with the well known "composite spheres assemblage": an isotropic sphere p is enclosed in an isotropic concentric shell m. The use of variational principles leads to Hashin and Shtrikman's bounds [9] which show that only the volumic fractions and the moduli of each phase are needed to predict the overall Young's modulus. For a two-phase material, the lower bounds for effective bulk (K_v) and shear (G_v) moduli can be calculated according to:

$$K_v^- = K_m + \frac{v_p}{\frac{1}{(K_p - K_m)} + \frac{3\cdot v_m}{(3\cdot K_m + 4\cdot G_m)}} \tag{5}$$

$$G_v^- = G_m + \frac{v_p}{\frac{1}{(G_p - G_m)} + \frac{6\cdot(K_m + 2\cdot G_m)\cdot v_m}{5\cdot G_m(3\cdot K_m + 4\cdot G_m)}} \tag{6}$$

The lower bound of the Young's modulus is given by:

Table 3 Comparison of real and simulated cross-sections

Surfacic fraction S_p	7.2%	27.6%	48.1%
Cross-section of real sample			
Simulated cross-section			

$$E_v^- = \frac{9K_v^- G_v^-}{3K_v^- + G_v^-} \quad (7)$$

The m, p and v subscripts denote matrix, inclusions and two-phase material respectively. The upper bound is obtained by interchanging m and p subscripts in Eqs. 5 and 6.

Construction of the two-dimensional numerical model

The preliminary work before simulation consists to build a geometrical model for two-phase materials enclosing spherical inclusions randomly distributed in the matrix. In order to lead to confident Young's modulus values, this model must exhibit a good representativeness of the actual material microstructure, chiefly dealing with dimensions, geometry and spatial second phase distribution. Consequently, the best solution consists to develop 3D models [10, 11]. Unfortunately, this approach often needs a large duration of pre-processing and computation. Among two-dimensional approaches, boundary integral methods were developed by Mogilevskaya and Crouch [12–14] for circular inclusions. On the other hand, for some three-dimensional arrangements, the problem can be advantageously reduced to a 2D one by considering cross-sections representative of the whole sample from a stereological point of view. Indeed this approach requires acceptable times of calculation and so permits to increase the number of studied parameters. Thus, it has been used for this work. The method implemented uses mathematical relationships suggested by Fullman [15] to reconstruct spheres from circles obtained from a random cut. The stereological relationships, which are commonly used in image analysis, ensure the passage from a 2D system to a 3D one (and vice versa). They allow to calculate from a statistical viewpoint the 2D diameter distribution (in number) of the sections of spheres. Thus the representativeness of the 3D material is respected. Indeed, King [16] so as Garboczi and Roberts [17, 18] have used some of these methods of statistical re-build for two-phase materials with random structure. They implement Boolean models and use the ''Identical Overlapping Sphere'' procedure. On the contrary, this work deals with spheres fully disconnected ones from each others. So, the use of numerical simulation needs for pictures of sample cross-sections compatible with the MEF software pre-processors capabilities. A random cut in the bulk of a model sample shows the sections of alumina balls, the diameters of these sections lying between 0 and the diameter of the largest ball. One way consists to digitize the picture obtained by sectioning a real sample [19, 20]. Then, specific software of contour recognition permit the meshing of such pictures after quantification in gray levels. Our first uses of this method show that the quality of results depends closely on the pictures quality (fine polishing of the face, high image resolution and efficiency of the software of contour recognition). The original character of the method here developed is that it reconciles both the speed of calculation and a good representativeness of the 3D materials reality by taking into account stereological relationships: the sections of spherical inclusions are generated in an automatic way and all the operating conditions are user-definable.

Description of the method

The method used to generate 2D cuts is based on the works carried out by Watson [21] on the reconstitution of spheres starting from the circles induced by the cut. The expressions allowing the passage from a 3D to a 2D system are valid for homeomorphic and convex 3D particles only. The sphere being the simplest convex particle, inclusions are considered as perfect spheres although some of them can exhibit slightly different geometry (Fig. 1). To predict the 2D distribution of the sphere sections, the knowledge of the real 3D distribution of their diameters is needed [22]. The Fig. 1 shows the granulometric curve of the alumina balls (by number) obtained by image analysis [size range: D_{10} = 1.26 mm, D_{50} = 1.41 mm and D_{90} = 1.57 mm]. It is possible [23] but more complicated to take into account the real granulometry during the 3D to 2D passage. So in order to simplify calculations, a single mean diameter D equal to the D_{50} value of the

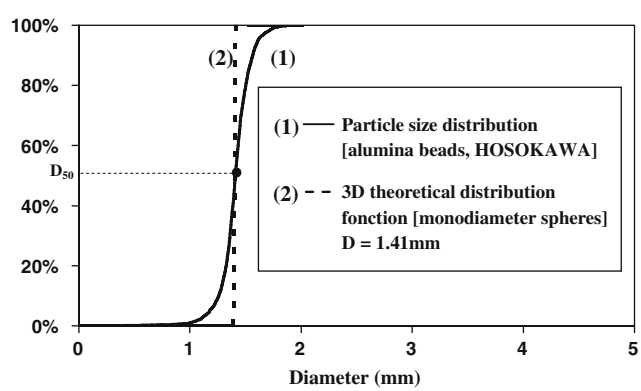

Fig. 4 Approximation of the actual granulometric curve for alumina beads

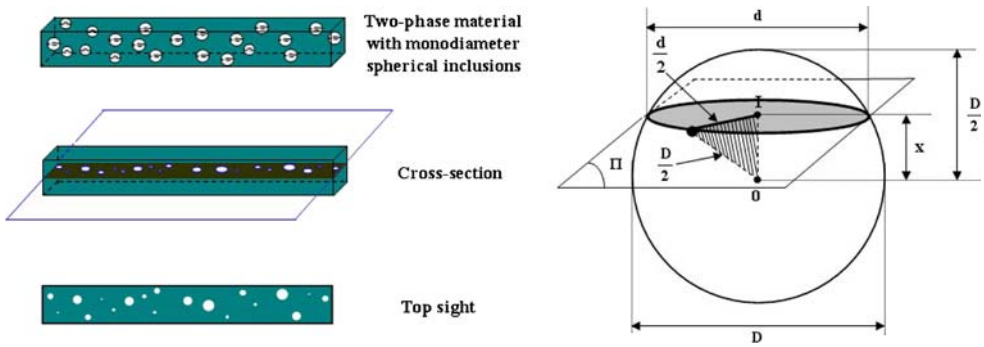

Fig. 5 Geometrical relationships in a sphere randomly cut by a plane

granulometric curve was selected (Fig. 4). The rather narrow balls granulometry distribution justifies such an assumption.

Building of the two-dimensional numerical model from the theoretical distribution function F(d)

The Fig. 5 represents a cut plane Π at an arbitrarily altitude x: this cut can or cannot intercept inclusions. If a sphere randomly located regarding Π is intercepted, the center I of the resulting circular section is at the distance x from the center O of the sphere. When x varies from 0 to D/2, the theoretical distribution function $F(d)$ corresponding to the equiprobability to find a section diameter lower than d can be written:

$$F(d) = 1 - \frac{2}{D}\sqrt{\left(\frac{D}{2}\right)^2 - \left(\frac{d}{2}\right)^2} \tag{8}$$

The simulated sections have a perfect circular geometry. The sum of their individual surfaces gives the 2D surfacic fraction which agrees with the 3D content chosen for a given sample. Thus, this parameter is fully controlled.

For low contents, the number of sections remains relatively low and the corresponding section diameter distribution function is then rather far from the theoretical $F(d)$ curve. On the other hand, in the case of significant contents, the two distribution functions tend to be superimposed because of the increase in the number of sections. Moreover, a truncation of the curve $F(d)$ is needed to insure that the diameter of the smallest section is compatible with the capabilities of the FEM software (meshing capacities and calculation duration).

The Table 3 allows to compare, 2D cuts of real material and corresponding 2D numerical cuts for the same volumic content ($D_{\text{inclusions}}$ = 1.41 mm). A very good agreement is observed even if any virtual inclusion cut does not intercept the edges of the sample or another inclusion (for numerical conveniences).

The original program for automatic generation of virtual sections creates geometrical D×F files. All the geometrical and numerical parameters are adjustable, as well as the truncation defining the smallest acceptable diameter (Fig. 6). In a first time, the capabilities of four FEM software (ABAQUS, ALGOR, NISA and RDM Le-Mans) were compared on two 2D models (Table 4). The obtained results being identical with a scattering less than 0.5%, the fastest and powerful of them (RDM Le-Mans) was then systematically used for all calculations. The good effectiveness of RDM Le-Mans is improved by using an optimized design of the program of sections generation supplying files directly compatible with the automatic meshing module.

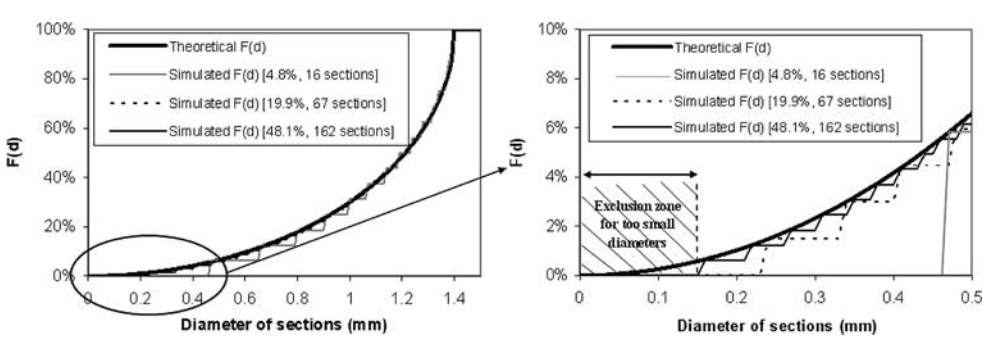

Fig. 6 Truncation of the real $F(d)$ curve dealing with the distribution function of simulated sections

Table 4 Young's modulus values calculated using 4 FEM software (for 2 different cross-sections)

	RDM Le-Mans V. 5	ALGOR V. 15.0	NISA V. 7.0	ABAQUS V. 6.1
Type of elements	6-TR	3-TR + 4-QUAD	6-TR + 8-QUAD	6-TR
Simulated cross-section			s_p = 9.5%	Number of balls = 11
Number of elements	314	1,550	1,220	2,453
Duration of pre-processing	1 min	30 min	45 min	30 min
Duration of computation	3 s	4 s	10 s	1 min 30 s
E value (GPa)	86.81	86.62	86.60	86.69
Maximum variation	0.25%			
Simulated cross-section			s_p = 30.5%	Number of balls = 36
Number of elements	1,034	4,862	3,414	6,250
Duration of pre-processing	1 min	1 h 30	2 h 00	1 h 30
Duration of computation	5 s	7 s	1 min 30 s	4 min
E value (GPa)	105.70	105.54	105.67	105.64
Maximum variation	0.16%			

3-TR: 3 nodes-triangular elements6-TR: 6 nodes-triangular elements with 6 nodes4-QUAD: 4 nodes-quadrangular elements8-QUAD: 8 nodes-quadrangular elements

Finite element calculation

The numerical estimation of Young's modulus uses the FEM simulation of a pure tensile test of a sample subjected to applied stresses (Fig. 7). The material behavior is supposed elastic linear according to the Hooke's law.

All nodes located in the cross-section at the origin of the sample are fully fixed along the x-axis and one of them has null DOF along the y-axis. The cross-section at the extremity of the sample is subjected to a constant stress σ. Calculation, performed in plane stress state, leads to the mean displacement ΔL of all the nodes of the stressed surface and then to the elastic modulus along the loading direction. Care in modeling is needed because the result may be dependant both on the meshing density and on the type of element used [24]. A preliminary study has shown that for 2D cuts, the inclusions periphery must be quantified by 8 nodes at least. A lower value decreases slightly the overall rigidity and thus leads to a lower estimated modulus, a greater value does not improve significantly the final result. The automatic meshing is carried out using 6 nodes triangular elements well suited to describe curved lines. Because of the random location of inclusions within the sample, results can vary from a sample to another exhibiting similar volumic content. In order to limit the effects of such statistical variations, 6 pure tensile tests have been simulated on 6 different samples for each content value.

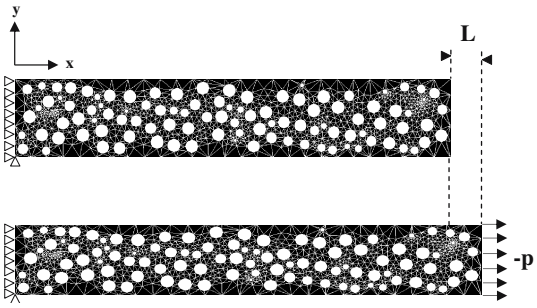

Fig. 7 FEM modeling of a pure tensile test

Results and discussion

The numerical values used in simulation for the elastic properties of the two phases have been experimentally measured (E_m = 78 GPa, ν_m = 0.21, E_p = 240 GPa) and Poisson's ratio of alumina is supposed close to 0.24. These same data also allow to perform analytical calculation.

The Table 5 summarizes all the Young's modulus values ranked by increasing contents. Because inclusions are randomly located in simulated sections, the real content is never exactly equal to its expected value. So, after computerized generation of inclusions, it is accurately calculated for each sample.

One observes on Fig. 8 that E increases when the inclusions content increases and that these values are very close to the lower Hashin and Shtrikman's bound:

Table 5 Summary of Young's modulus values

Experimental		Numerical		Analytical			
US measurements		2D simulation		Voigt	Reuss	Hashin and Shtrikman	
v_p (%)	E (GPa)	s_p (%)	E (GPa)	E (GPa)	E (GPa)	E^- (GPa)	E^+ (GPa)
0	78.0	0	78.0	78.0	78.0	78.0	78.0
–	–	4.8	81.6	85.8	80.6	81.9	83.3
5.0	81.9	–	–	86.1	80.7	82.1	83.5
–	–	–	–	86.4	80.8	82.2	83.7
–	–	6.9	83.2	89.2	81.8	83.7	85.6
7.5	84.6	–	–	90.2	82.2	84.2	86.3
–	–	9.9	85.6	94.0	83.6	86.3	89.0
–	–	–	–	94.8	83.9	86.7	89.6
–	–	12.0	87.3	97.4	84.9	88.2	91.5
13.0	89.7	–	–	99.1	85.5	89.1	92.6
–	–	14.9	89.7	102.1	86.7	90.8	94.9
–	–	–	–	102.8	87.0	91.2	95.4
–	–	19.9	94.1	110.2	90.1	95.6	100.9
20.0	96.8	–	–	110.4	90.2	95.7	101.1
–	–	–	–	110.7	90.3	95.9	101.3
–	–	24.9	98.8	118.3	93.8	100.7	107.2
–	–	–	–	118.5	93.8	100.8	107.4
–	–	26.9	100.8	121.6	95.3	102.8	109.8
–	–	–	–	121.9	95.5	103.0	110.1
28.0	106.3	–	–	123.4	96.2	104.0	111.2
–	–	34.9	109.3	134.5	102.0	111.7	120.5
35.0	113.9	–	–	134.7	102.1	111.9	120.7
47.0	129.5	–	–	154.1	114.2	127.1	138.0
–	–	48.0	125.1	155.8	115.4	128.5	139.6
–	–	54.7	134.5	166.6	123.7	138.3	150.1
55.0	140.6	–	–	167.1	124.1	138.7	150.6

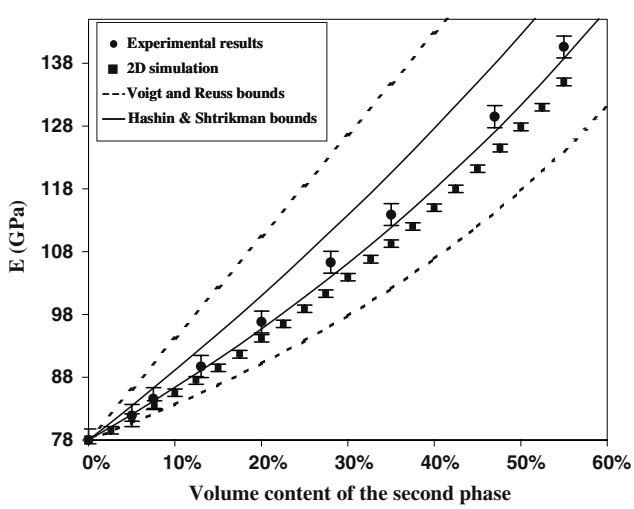

Fig. 8 Comparison between experimental, numerical and analytical Young's modulus results

- the maximum difference $\Delta E/E$ between this bound and values given by the numerical simulation does not exceed 2.8% for the highest studied content (54.7 vol%).
- the dispersion $\gamma = (E_{min}–E_{max})/E_{average}$ calculated for the 6 cuts of the same 2D content is lower than 1.1%.

So, the local statistical fluctuations due both to the random location of inclusions and to their eventual rough modeling (smallest objects) are thus strongly limited.

Finally, it has been observed that results appear not dependant on the fact that inclusions cut or do not cut the sample faces but that the scale factor can induce significant errors since the number of 2D inclusions becomes low.

Conclusion

The three approaches implemented in this work (analytical, experimental and numerical) to estimate the elastic properties of a two-phase material lead to quite similar Young's modulus values, close to the lower bound of the analytical Hashin–Shtrikman's model. Indeed, this model seems to give the best approximation of granular materials behavior including particles more rigid than the matrix when information on phase volumic fractions is considered only [25]. However, it becomes quickly more and more complex since one considers more than three phases. Moreover, interfacial disagreements between phases

are difficult to take into account with analytical approaches. It is from these points of view (materials with complex microstructures) that the numerical simulation exhibits a major interest.

For the present 2D study, cuts of material have been simulated by software: they are representative of a two-phase material including mono-diametral spheres randomly dispersed in the bulk. But they can be considered also as representative of cross cuts of mono directional composite materials including long cylindrical fibers of various diameters randomly dispersed in the bulk along a given direction. This duality could partly explain the systematic under-estimate of the effective 2D Young's modulus and it may be thought that more realistic 3D modeling leads to more significant values. But this latter implies more delicate analysis and requires rather long computational treatments.

Considering the limited error induced by 2D analysis and the fastness of calculation, it can be conclude that, from a practical point of view, 2D modeling is a good tool to predict the effective Young's modulus of multiphased materials and that 3D modeling can be performed when high accurate results are needed.

References

1. Burr A, Schmitt N, Berthaud Y (1993) Int. seminar on micromechanics of materials, 6–8 July 1993. MECAMAT93, Moret-sur Loing, France, pp 436–447
2. Coster M, Chermant JL (1989) Précis d'analyse d'images. Edition du CNRS, Paris
3. Cutard T, Fargeot D, Gault C, Huger M (1994) J Appl Phys 75:1909
4. Asmani M, Kermel C, Leriche A, Ourak M (2001) J Eur Ceram Soc 21:1081
5. Glandus JC (1981) Rupture fragile et résistance aux chocs thermiques de céramiques à usage mécanique. PhD thesis, University of Limoges
6. Voigt W (1910) Lehrbuch der Kristallphysik. Teubner, Berlin
7. Reuss A (1929) Z angew Math u Mech 9:49
8. Hashin Z (1962) J Appl Mech 29:143
9. Hashin Z, Shtrikman S (1963) J Mech Phys Solids 11:127
10. Sangani AS, Mo G (1997) J Mech Phys Solids 45:2001
11. Kushch VI (1997) Int J Solids Struct 34:1353
12. Mogilevskaya SG, Crouch SL (2001) Int J Numer Methods Eng 52:1069
13. Crouch SL, Mogilevskaya SG (2003) Int J Numer Methods Eng 58:537
14. Mogilevskaya SG, Crouch SL (2004) Int J Numer Methods Eng 41:1285
15. Fullman RL (1953) Trans AIME J Met 5:447
16. King RP (1996) Chem Eng J 62:1
17. Roberts AP (1997) Phys Rev E 56:3203
18. Roberts AP, Garboczi EJ (1999) J Mech Phys Solids 47:2029
19. Zhonghua L, Haicheng G (1990) Met Trans 21:717
20. Jaensson BO, Sundström BO (1972) Mat Sci Eng 9:217
21. Watson GS (1971) Biometrika 58:483
22. Xu YH, Pitot HC (2002) Comput Methods Progr Biomed 00:1
23. Sahagian DL, Proussevitch AA (1998) J Volc Geo Res 84:173
24. Ankem S, Margolin H (1982) Met Trans 13:595
25. Watt JP, O'Connell RJ (1980) Phys Earth Planet Int 21:359